Lab Notes

Editors
Thomas M. Moses | Shane F. McClure

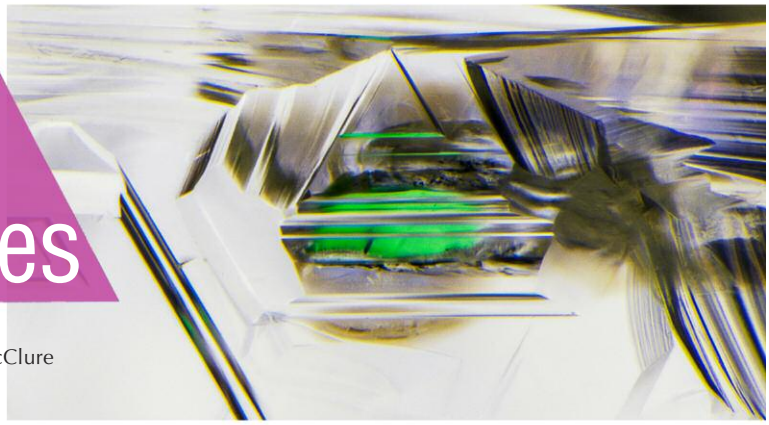

Resin-Coated and Clarity-Enhanced AQUAMARINE Pendant

The Carlsbad laboratory received a 34.24 ct light greenish blue free-form pendant (figure 1) measuring 33.40 × 25.75 × 6.40 mm. One side of the pendant was flat and polished, and the other side had a rough surface. Standard gemological testing gave a refractive index (RI) of 1.570–1.580. The pendant had the same reaction to long-wave and short-wave UV light: blue fluorescence in the center and green fluorescence around the edges of the stone. Examination with a standard gemological microscope revealed a blue and orange flash effect most clearly visible from the flat side (figure 2, left), which is diagnostic of clarity enhancement. Ultraviolet/visible/near-infrared (UV-Vis-NIR) spectra were consistent with natural aquamarine, with absorption peaks at 370 and 425 nm and an absorption band at ~830 nm (figure 2, right). Raman spectroscopy showed the presence of polymer on the rough side of the stone and aquamarine on the polished flat side. Although emeralds are the variety of beryl most commonly associated with clarity enhancement, filled aquamarine has previously been reported in the Chinese market (J. Li et al., "Polymer-filled aquamarine," Fall 2009 *G&G*, pp. 197–199).

Figure 1. This 34.24 ct light greenish blue free-form aquamarine pendant, measuring 33.40 × 25.75 × 6.40 mm, was seen in the Carlsbad laboratory. Stone courtesy of Stephen Challener.

Only one side, the rough side, was coated with polymer resin. Viewed in the microscope, this side appeared to have a thin transparent layer on the surface. Trapped air bubbles were visible with magnification (figure 3, left), and areas with the coating had a higher luster than the polished flat side. Fourier-transform infrared (FTIR) spectroscopy taken from the rough side revealed strong diagnostic peaks at ~3100–2850 cm^{-1} (figure 3, right).

Although clarity enhancement and coating of beryl gemstones are

Editors' note: All items were written by staff members of GIA laboratories.

Gems & Gemology, Vol. 55, No. 2, pp. 246–259.

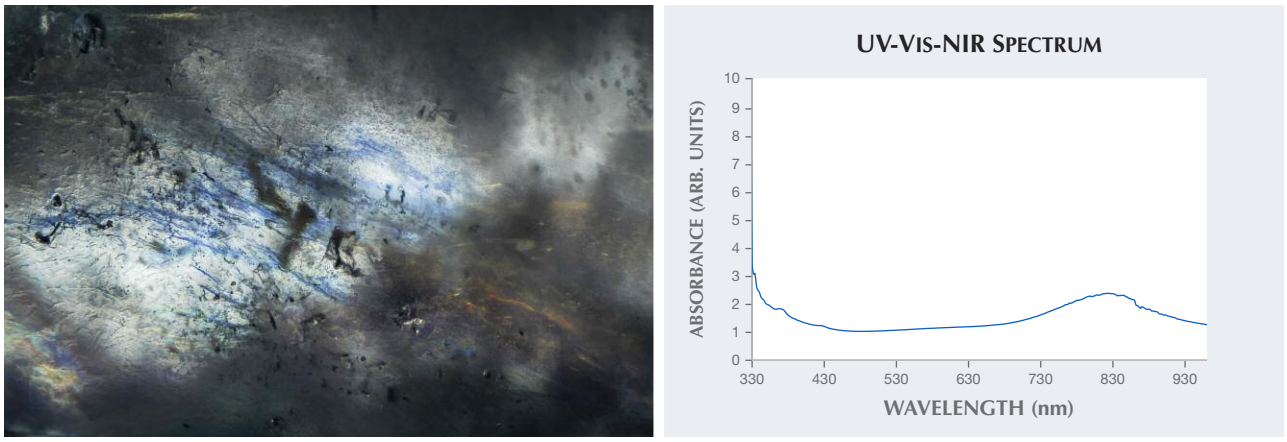

Figure 2. Left: The orange and blue flash effect seen in a clarity-enhanced fracture of the aquamarine; field of view 4.24 mm. Right: The UV-Vis-NIR spectrum, with absorption peaks at 370 and 425 nm and an absorption band at ~830 nm, is consistent with natural aquamarine.

not uncommon, this material is rarely seen in a gemological laboratory. Both treatments are readily identified, but careful examination of every stone is important to identify them.

Michaela Stephan

Rough DIAMOND Crystal with an Unusual Coating of Fake Green "Radiation Stains"

Due to their rare occurrence and the environment required to create their color, natural green diamonds are some of the world's most beautiful and sought-after gems. Most diamonds acquire their color from impurities or defects incorporated into the diamond lattice when the material is hundreds of kilometers deep in the earth's mantle. But most natural green diamonds are colored by radiation damage that occurs at very shallow depths in the earth's crust over long periods of time. Commonly accompanying this exposure to radioactive minerals and fluids are surface patches of green or brown color that gemologists call "radiation stains." These are simply areas of extreme damage to the diamond structure caused by alpha particle radiation. Initially green, they turn brown immediately after exposure to temperatures above 500°C. These surface features indicate that a diamond has been exposed to a source of natural radiation; green stains are commonly associated with naturally colored green diamonds.

Recently, GIA's Carlsbad laboratory examined an interesting attempt to imitate a natural green diamond when a 6.49 ct green crystal was submitted for a Colored Diamond Grading Report (figure 4). The surfaces of the resorbed octahedron were covered by uneven patches of green color. Fourier-transform infrared (FTIR) analysis revealed a typical type Ia diamond with abundant nitrogen and hydrogen impurities. However, the ultraviolet-visible (UV-Vis) spectrum was very unusual and did not show any of the bands that are produced by radiation damage in diamond (e.g., the

Figure 3. Left: Gas bubbles and high luster on the aquamarine's resin-coated rough surface, shown near the drill hole. Field of view 7.19 mm. Right: The FTIR spectrum shows polymer peaks at ~3100–2850 cm^{-1}. The dotted line is the spectrum of an untreated aquamarine, shown for reference.

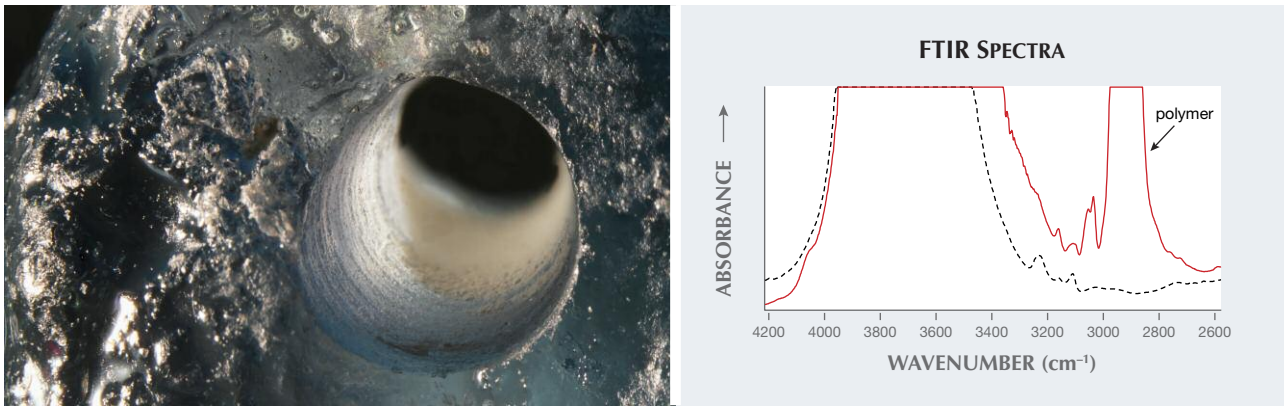

Figure 4. This 6.49 ct rough diamond with patchy green surface color was submitted to GIA's Carlsbad laboratory for a Colored Diamond Grading Report.

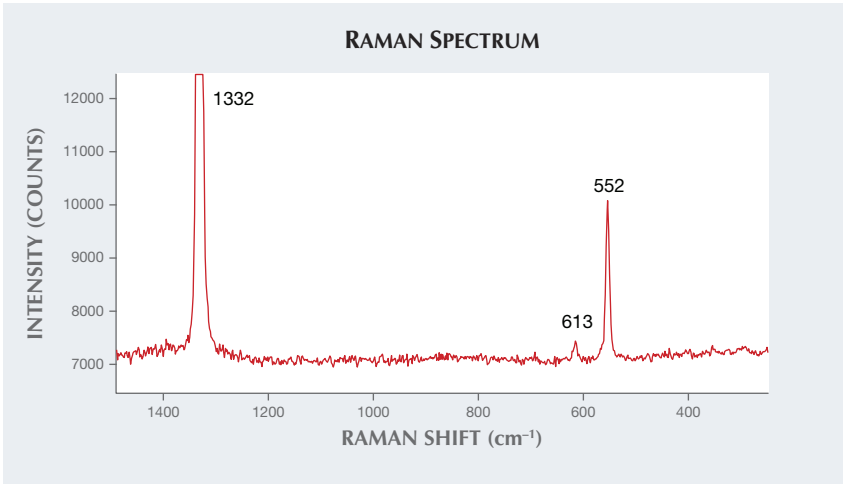

Figure 6. The Raman spectrum (514 nm laser excitation) of the rough diamond's green coating shows clear peaks from chromium oxide (552 and 613 cm^{-1}) as well as the underlying diamond (1332 cm^{-1}). The specific positions of the chromium oxide peaks suggest the coating has been annealed to ~700°C (Mohammadtaheri et al., 2018).

GR1 defect). Careful examination under magnification found that the green color was not due to radiation stains, but instead to groupings of emerald-green platy crystals, ~40 µm in size, attached to the diamond surface (figure 5). Individual platy crystals could easily be flaked off using tweezers or a pointer probe, but they remained adhered to the surface under normal gem testing situations, including wiping the diamond with a stone cloth. X-ray fluorescence (XRF) analysis indicated high concentrations of chromium, and Raman analysis identified the green plates as chromium oxide (figure 6). The Raman peak positions correlated very well with chromium oxide powder that had been heated to ~700°C to produce a crystallized coating (M. Mohammadtaheri et al., "The effect of deposition parameters on the structure and mechanical properties of chromium oxide coatings deposited by reactive magnetron sputtering," *Coatings*, Vol. 8, No. 3, 2018, Article No. 111). A small H1b defect present in the diamond's FTIR spectrum supports this annealing temperature.

Figure 5. The diamond's patchy green coloration is caused by interlocking platy crystals of chromium oxide, visible with magnification. Field of view 0.72 mm.

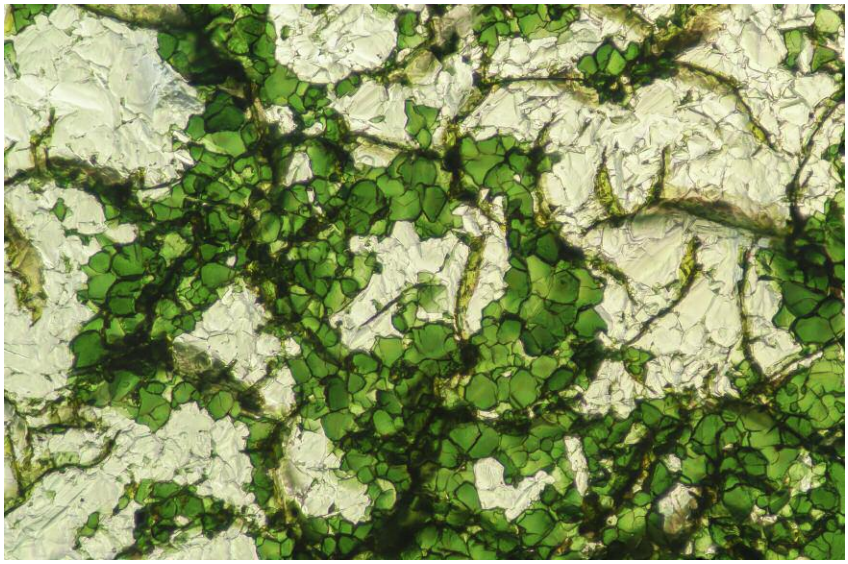

Most colored coatings encountered in the lab are on faceted stones and are pink, orange, red, or blue. The warmer hues are typically created by sputter-coating techniques involving metals and the colder hues by inks or other organic dyes. The use of chromium oxide powder to produce a green coating—along with annealing of the powder to produce crystallized plates that adhere to the rough surface to resemble radiation stains—represents a significant attempt to artificially reproduce the features seen on natural green diamonds. While the unique coating is easily discerned from natural green radiation stains under magnification, this stone is a strong reminder to carefully examine any green diamond,

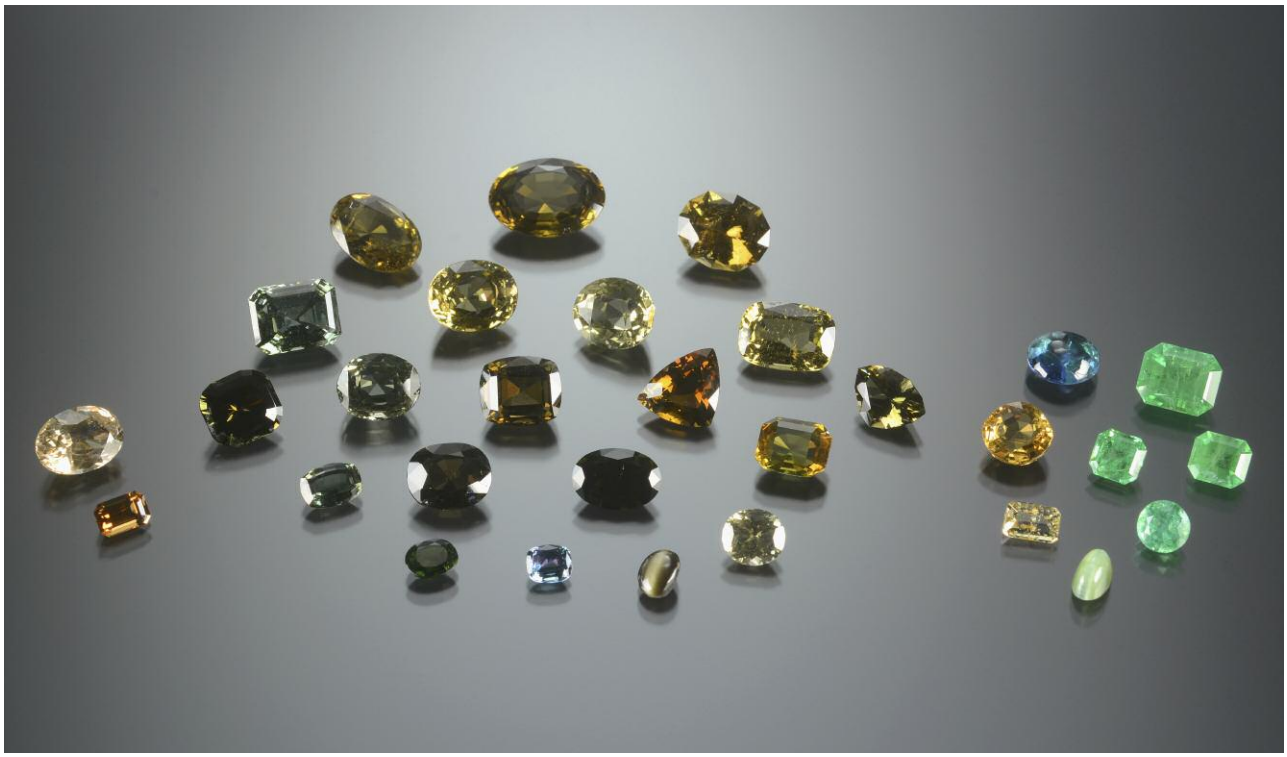

Figure 7. The two stones on the far left, corresponding to the blue analytical points in figure 8, were classified as kornerupine. The center 20 stones, corresponding to the yellow analytical points in figure 8, were classified as prismatine. For the eight stones on the right, corresponding to the red analytical points, the species could not be determined. The species classifications of all the stones were based on chemistry acquired by LA-ICP-MS. The largest stone is the 11.9 ct brown oval at the top of the center group. The smallest is the light blue cushion stone at the bottom of the center group, weighing 0.93 ct.

even rough crystals, in order to know exactly what you are buying.

Virginia A. Schwartz and Christopher M. Breeding

Separation of KORNERUPINE and PRISMATINE

Kornerupine and prismatine form a solid solution series with a general chemical formula of $^{X}(\square,Mg,Fe)\,^{M}(Al,Mg,Fe)_9\,^{T}(Si,Al,B)_5(O,OH,F)_{22}$ (X: cubic site; M: octahedral sites; T: tetrahedral sites). Chemically, they differ mainly in magnesium, iron, aluminum, and fluorine content, with boron content that ranges from 0 to 1 apfu (atoms per formula unit) in one of the tetrahedral sites. When the boron apfu is less than 0.5, the mineral is classified as kornerupine; above 0.5, it is classified as prismatine (E.S. Grew et al., "Prismatine: revalidation for boron-rich compositions in the kornerupine group," *Mineralogical Magazine*, Vol. 60, No. 400, 1996, pp. 483–491).

GIA laboratories have recently implemented a method using laser ablation–inductively coupled plasma–mass spectrometry (LA-ICP-MS) to quantify boron concentration in kornerupine and prismatine in order to distinguish the two. The 30 stones shown in figure 7—all thought to be kornerupine—were borrowed from the GIA Museum and tested using a Thermo Fisher iCAP Qc ICP-MS, coupled with an Elemental Scientific Lasers NWR213 laser ablation system. GSD-1G and GSE-1G (U.S. Geological Survey) and NIST 610 were used as external standards. ^{29}Si was used as an internal standard. Three 55 µm circular spots were ablated on the girdle of each stone. The data reduction was a modified version of that used at GIA for tourmaline (Z. Sun et al., "A new method for determining gem tourmaline species by LA-ICP-MS," Spring 2019 *G&G*, pp. 2–17). As a result, we have slightly modified the criteria for separating the two to account for analytical error. If the boron apfu is between 0 and 0.45, the stone is classified as kornerupine. Between 0.45 and 0.55 apfu, the species cannot be determined by this method. If the boron apfu is between 0.55 and 1, the stone is classified as prismatine. For three spot analyses, if one spot has a boron apfu between 0.45 and 0.55, the species is undetermined.

All analytical points were plotted in figure 8 (full chemical results are in appendix 1 at www.gia.edu/gems-gemology/summer-2019-labnotes-separation-kornerupine-prismatine-appendix1.pdf). There were 2 kornerupine, 20 prismatine, and 8 undetermined species, for a total of 30 tested stones. This result suggests that, contrary to popular belief, prismatine may

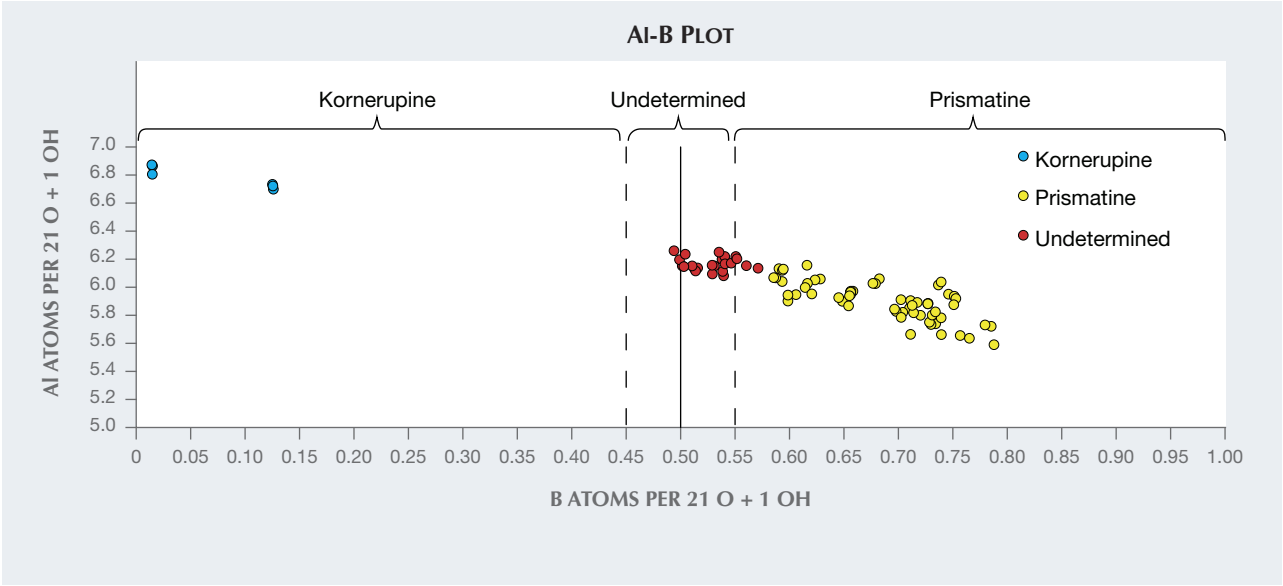

Figure 8. The Al-B plot shows three sections. When the B (apfu) is between 0 and 0.45, stones are classified as kornerupine (blue spots). When the B (apfu) is between 0.45 and 0.55, the species for the stones (red spots) cannot be determined. When the B (apfu) is between 0.55 and 1.00, stones (yellow spots) are classified as prismatine. For three spot analyses, if one spot has a B (apfu) between 0.45 and 0.55, the species is considered undetermined.

be a far more common gem species than kornerupine, which is also supported by the analyzed boron concentration of many production stones submitted to GIA laboratories. Interestingly, for the five green stones tested here the species could not be determined, although they slightly favor prismatine chemistry (some of the red spots in figure 8). Aluminum apfu is also a good indicator for separating kornerupine from prismatine. Boron-rich prismatine has an Al apfu around 5.8 to 6.0, compared to boron-poor kornerupine with an Al apfu around 6.6 to 6.8. Extra Al in kornerupine functions as a substitute for B in one of the tetrahedral sites in the crystal lattice.

Kornerupine is an appropriate group name for kornerupine-structure minerals of an unknown boron content or for cases where the species cannot be determined. For extreme cases, such as when boron apfu is close to 0 or 1, Raman spectroscopy could be sufficient to separate kornerupine from prismatine (B. Wopenka et al., "Raman spectroscopic identification of B-free and B-rich kornerupine (prismatine)," *American Mineralogist*, Vol. 84, No. 4, 1999, pp. 550–554). However, the more accurate separation for the two is determined by LA-ICP-MS analysis because the species definition is based on concentration of a chemical element, boron.

Ziyin Sun, Jonathan Muyal, Nathan D. Renfro, Shane F. McClure, and Aaron C. Palke

Faceted MILARITE

Recently the Carlsbad lab received a light yellow 2.07 ct unknown gemstone (figure 9). The measured refractive index was 1.548–1.550 with a birefringence of 0.002. The specific gravity, measured hydrostatically, was

Figure 9. This 2.07 ct oval brilliant is the first faceted milarite examined by the Carlsbad lab.

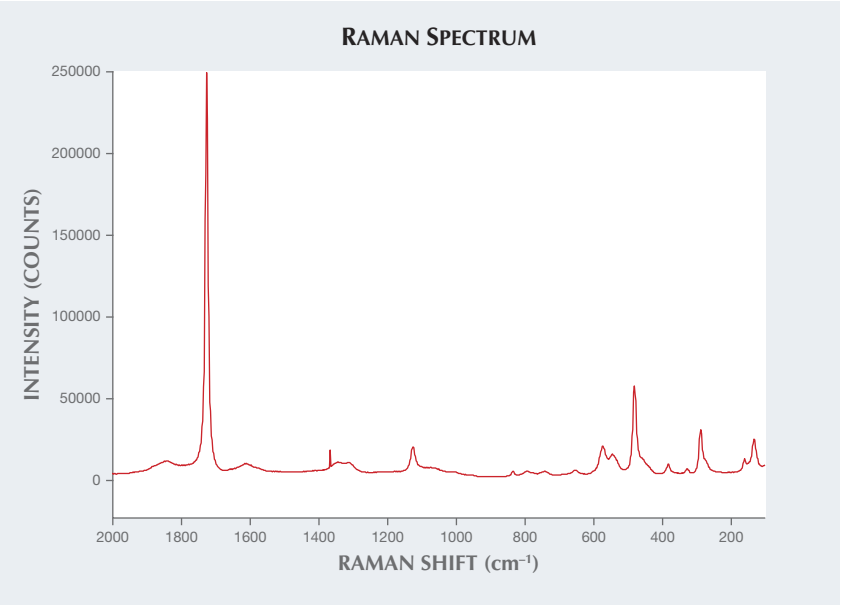

Figure 10. Raman spectroscopy confirmed the gem to be milarite.

2.52. These properties were consistent with the mineral milarite, which was confirmed by Raman spectroscopy (figure 10). The stone showed planar/patterned liquid inclusions resembling a honeycomb pattern and also contained needle-like inclusions.

Milarite is fairly rare but gives its name to a somewhat large group of silicates, namely the milarite-osumilite group. This group is composed of similar cyclosilicate minerals that are very rare and obscure. Crystals are generally small and often have a muted green or yellow color, and they occur as well-formed prismatic hexagonal crystals. Milarite is a hexagonal-dihexagonal dipyramidal mineral with a composition of $K_2Ca_4Al_2Be_4Si_{24}O_{60}\cdot H_2O$. It forms as a primary mineral in granitic pegmatite, low-temperature hydrothermal veins, and alpine clefts.

The mineral was named by Gustav Kenngott (1870) after he mistakenly identified its provenance as Val Milar, located in eastern Switzerland. The original specimens actually came from neighboring Val Giuf. Even though milarite was the first newly described mineral from a Swiss Alpine fissure, it took more than 60 years to identify the mineral's true chemical nature, in particular its Be content. Milarite was originally known as a green mineral, until fine yellow crystals were discovered in Mexico in 1968. Larger Mexican crystals with transparent areas have occasionally been faceted into small gems with a pleasing appearance, but these are exceedingly rare.

Outside of Switzerland, notable occurrences have been recorded in Brazil, Mexico, Germany, Russia, Canada, Italy, Norway, and the Czech Republic. Nevertheless, this is the first example of faceted milarite ever examined by the Carlsbad laboratory.

Forozan Zandi

A "Hollow" PEARL Filled with Foreign Materials

The interior structures of pearls are always of interest, as they are never revealed until the analysis begins. External appearance may provide experienced pearl testers with some clues on what to expect when microradiography commences, but sometimes the structure revealed is beyond expectation (Spring 2014 Lab Notes, pp. 66–67; Winter 2015 Lab Notes, pp. 434–436).

In early 2019, a semi-baroque white and cream pearl, weighing 28.49 ct and measuring 19.23 × 16.44 × 15.05 mm (figure 11), was submitted to GIA's Bangkok laboratory. Its external appearance and size gave no obvious preliminary clues about its identity. A fairly small oval area on the base measuring approximately 5.20 × 3.10 mm differed in appearance from the rest of the pearl. Initial examination with a loupe and micro-

Figure 11. The submitted 28.49 ct pearl, alongside a Thai one-baht coin.

scope revealed that the pearl's surface had been worked and heavily polished, producing a lustrous appearance. Many surface areas had been modified, including the small oval area already mentioned. More detailed observation using a stereomicroscope revealed foreign materials within the yellow-brown area on the base (figure 12), including a piece of shell-like material (figure 12B and 12C, red arrows) together with other random fragments within a transparent light yellow substance enclosing several gas bubbles (figure 12D, blue arrows). Similar features were observed in the filler material used in natural blisters previously submitted to GIA (Summer 2016 Lab Notes, pp. 192–194). Although the surface structure indicated that the pearl was most likely filled with foreign materials, such an assumption could only be proved after more detailed study.

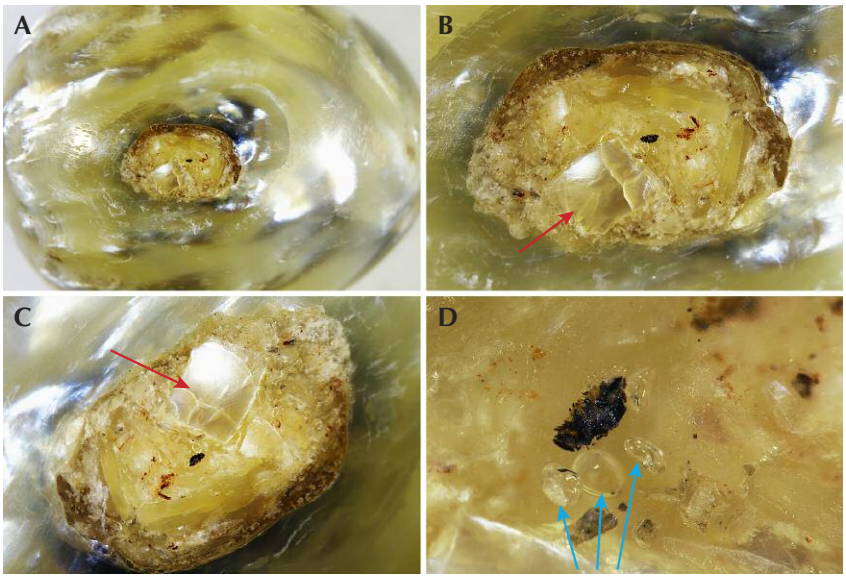

Figure 12. The pearl's base showing the filler (yellow-brown area) exposed at the surface (A). Field of view 19.20 mm. A magnified view of the filled area showing the largest shell-like material (B and C, red arrows) with other fragments within the transparent light yellow host filler. Field of view 7.20 mm. The gas bubbles in the filler are easily visible in this magnified view (D, blue arrows). Field of view 1.44 mm.

Real-time microradiography (RTX) and X-ray computed microtomography (μ-CT) revealed the pearl's internal structure, including a large dark and fairly irregular outline that indicates the pearl was hollow at one time. RTX analysis (figure 13A) showed that some parts of the structure clearly reached the surface at the base. After RTX examination in a number of different orientations, however, it was very apparent that the structure was no longer hollow. In-

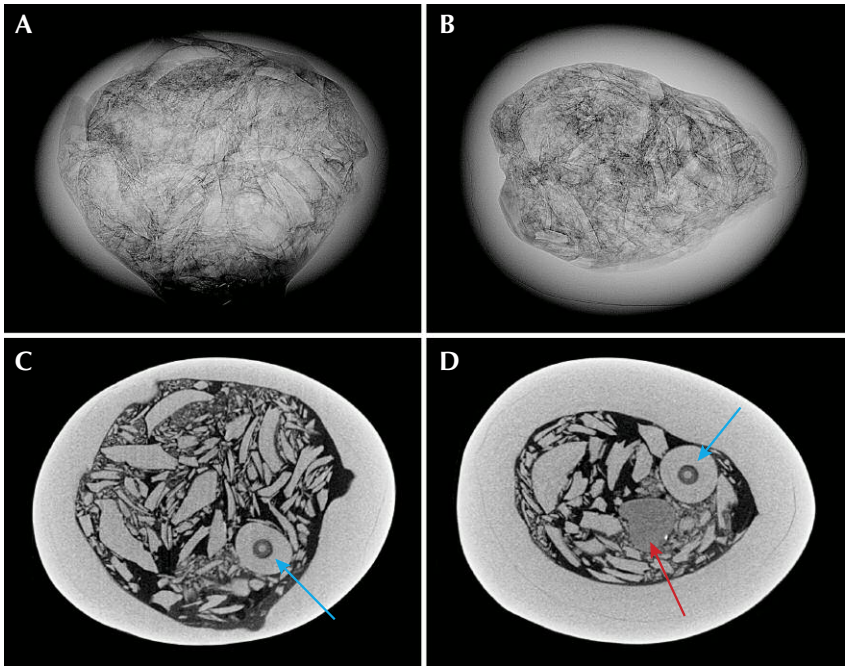

Figure 13. Top: Two RTX images reveal the complex internal structure observed in two different directions. Field of view ~21.19 mm. Bottom: Two μ-CT images reveal the structures in more detail. Field of view ~21.07 mm. The off-round features with a dark organic ring toward the center and a white core could be a natural seed pearl (C and D, blue arrows), while most of the other pieces seem to be fragments of shell. The identity of the more radio-translucent object (D, red arrow) with part of an additional white radio-opaque impurity within the filler is unknown and can only be solved through destructive testing.

stead, it was completely filled with foreign materials, displayed as an array of disorderly fragments (figures 13A and 13B). The µ-CT images revealed clearer structures, with the outlines of fragments in various sizes apparently suspended in the former void. The µ-CT results also showed a degree of structural variance in the materials present within the filler. One off-round feature displayed an organic-rich ring at its center, with a very small white core possibly indicating the presence of a small natural seed pearl (figure 13C and 13D, blue arrows). Other irregular features with a similar radio-opacity seemed to be related to pieces of shell (as seen with the microscope at the surface of the filled area on the base), while an unidentified, more radio-translucent feature was also noted (figure 13D, red arrow). An additional small radio-opaque white impurity (likely a metal fragment) was observed in association with the latter and may be seen with all the other components in the supplemental µ-CT videos (www.gia.edu/gems-gemology/summer-2019-lab-notes-hollow-pearl-filled-with-foreign-material).

The "hollow" form bears some similarity to previous cases, such as a natural hollow pearl (N. Sturman, "Pearls with unpleasant odors," GIA Laboratory, Bangkok, 2009, www.giathai.net/pdf/Pearls_with_unpleasant_odours.pdf) or the voids seen in some non-bead cultured pearls (N. Sturman et al., "X-ray computed microtomography (µ-CT) structures of known natural and non-bead cultured *Pinctada maxima* pearls," *Proceedings of the 34th International Gemmological Conference*, 2015, pp. 121–124). Nevertheless, we cannot be certain why this void was filled with a variety of materials. The most plausible reasons are that (A) the feature needed to be filled so the pearl could be used in jewelry, and a selection of natural "shell-related" materials were mixed with adhesive to achieve this goal, or (B) the process was carried out to add weight to the pearl so it could be sold for a higher price, or both.

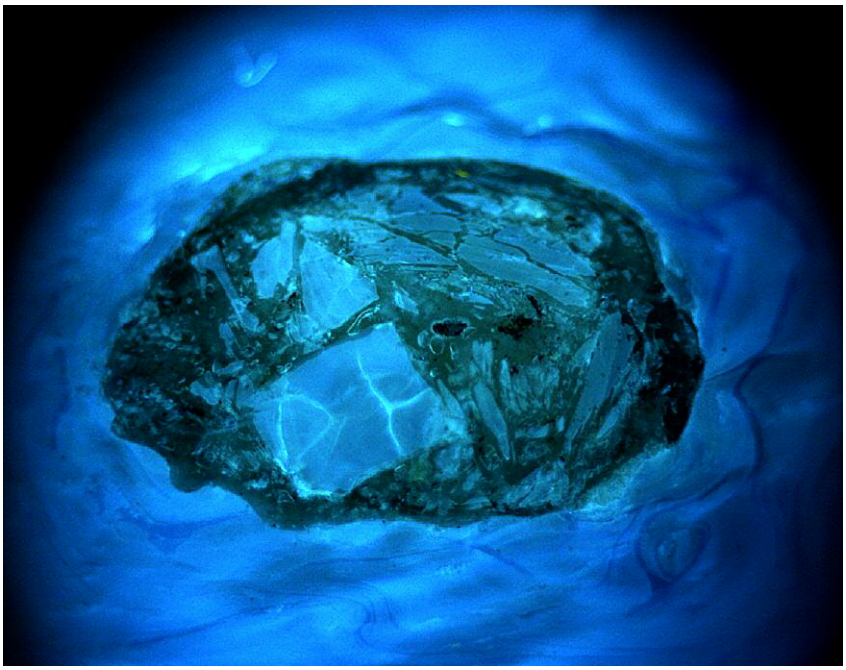

Figure 14. A strong blue fluorescence was visible on the pearl's surface under the DiamondView; the largest piece of shell and some of the smaller pieces with a matching appearance within the filler reacted in a similar manner. The other pieces in the filler exhibited slightly weaker reactions; the surrounding transparent filler showed a yellow-green color.

The pearl's fluorescence in the DiamondView was a strong blue, typical of many previously examined pearls. However, there was a degree of inhomogeneity that might be due to the surface condition (figure 14). The main reason to expose the pearl to the radiation of the DiamondView was to see how the materials in the filled area reacted. The results showed that the largest fragment and the pearl's surface produced a similar reaction, which supports the possible presence of shell pieces. Other smaller constituents showed weaker reactions, and the surrounding transparent host exhibited a yellow-green reaction.

Raman spectroscopic analysis of the filler confirmed the presence of shell based on a match with aragonite spectra, which is characteristic of many mollusks and pearls. The transparent filler material produced spectra that closely matched with a polymer. The chemistry of the largest piece of shell visible at the filler's surface was checked by energy-dispersive X-ray fluorescence (EDXRF) spectrometry and showed manganese (Mn) and strontium (Sr) levels characteristic of a saltwater environment.

Since the void within the pearl had been completely filled with foreign materials, it was unclear exactly what its original structure was prior to the work undertaken. Several scenarios are possible:

1. The pearl contained natural organic matter and formed naturally.
2. It had a large void with some organic matter in it, typical of some non-bead cultured pearls.
3. The large void contained a bead nucleus that was intentionally broken and mixed with bonding material and other components to fill the void and mask the identity, or the pieces of broken bead were removed before the void was filled with shell and other materials.

Figure 15. These two beads, 6.96 ct (left) and 2.25 ct (right), were identified as dyed serpentine.

Where doubt about the actual identity exists and each possibility has merit, it is unfair to the client to simply make an educated guess. After explaining the situation to the client, we left the identity of this pearl as "filled" but of an "undetermined" origin (natural, bead cultured, or non-bead cultured). Accordingly, a report was not issued.

Nanthaporn Nilpetploy

Dyed SERPENTINE Imitating Sugilite

The Carlsbad laboratory recently received a parcel of mottled purple beads (figure 15). A 2.25 ct translucent reddish purple broken bead from this parcel (shown on the right in figure 15) was examined for an identification report. At first glance, based on the color and structure, the sample resembled sugilite. Standard gemological testing revealed a refractive index of 1.56, a specific gravity of 2.71, weak orange fluorescence in both long-wave and short-wave UV, and a dye band with a handheld spectroscope. Sugilite has an RI of 1.607–1.610 and an SG of 2.74, and may show a concentrated band at 600 nm that can be confused with a dye band. The bead showed uneven color and a fibrous structure under the microscope (figure 16). There were no obvious dye concentrations, but the orange fluorescence and dye band in the spectroscope indicated the presence of dye. By performing a simple acetone test, we were able to prove that the material had been dyed. A light pink streak was examined after rubbing the test sample on a tissue soaked with acetone. The specimen's infrared spectrum was not consistent with sugilite but ended up matching well with serpentine. Chemistry collected via laser ablation–inductively coupled plasma–mass spectrometry (LA-ICP-MS) was consistent with serpentine, ruling out the possibility of sugilite.

Without advanced testing, it would have been difficult to conclusively identify this material as serpentine. This is the first time reddish purple dyed serpentine imitating sugilite has been examined in the Carlsbad laboratory, and gemologists should be aware of this imitation when examining sugilite.

Jessa Rizzo

Figure 16. The fibrous internal structure of the specimen resembling sugilite was actually consistent with serpentine. Field of view 4.11 mm.

Color-Change SPESSARTINE Garnet: A First Report

GIA's Carlsbad laboratory recently examined a 2.11 ct faceted stone (figure 17) that showed strong color change from dark green under daylight-equivalent lighting to dark red under incandescent illumination. Standard gemological testing revealed a refractive index that was over the 1.80 RI limit of the GIA desktop refractometer. This was the first example of a color-change garnet with an over-the-limit RI reading examined by GIA. Fluorescence was inert to long-wave and short-wave

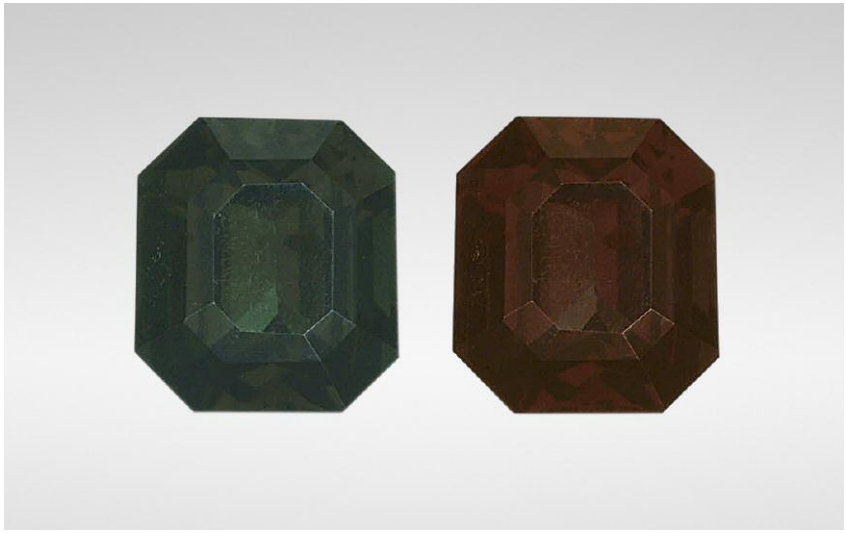

Figure 17. Color-change phenomenon was observed in this 2.11 ct octagonal mixed-cut spessartine. The left image, with a dark green color, was taken using an LED light source with 6500K color temperature (a daylight-equivalent light simulator). The right image, showing a dark red color, was taken with an LED light source with 2700K color temperature (an incandescent light simulator).

UV light. The stone did not show any pleochroism with the dichroscope. Using a handheld spectroscope, we observed a cutoff at about 460 nm and a broad band centered at about 575 nm. Microscopic examination revealed only a small fracture and strong internal strain. High-order interference colors were observed in cross-polarized light from the strain along grain boundaries.

Laser ablation–inductively coupled plasma–mass spectrometry (LA-ICP-MS) results showed that the stone was composed predominantly of spessartine (80.37 mol.%), with minor contributions from other end members of the garnet species (see table 1 at www.gia.edu/gems-gemology/summer-2019-labnotes-color-change-spessartine-garnet-icp-table1.pdf). It is classified as a spessartine garnet based on the criteria in the pyrope-spessartine-almandine ternary diagram (figure 18, left) modified from Stockton and Manson ("A proposed new classification for gem-quality garnets," Winter 1985 *G&G*, pp. 205–218). The RI and SG could also be calculated based on chemical composition (W.A. Deer et al., *Rock-Forming Minerals: Orthosilicates*, Vol. 1A, Geological Society of London, 1982, pp. 485–488).

Figure 18. Left: Three LA-ICP-MS data points, calculated based on molecular percentages for pyralspite garnet, were plotted in a pyrope-spessartine-almandine ternary diagram (modified after Stockton and Manson, 1985). Refractive index and spectral boundaries were used to distinguish among the six proposed garnet gem species labeled in the diagram. Right: The same data points were further plotted in the pyrope-spessartine-almandine RI-SG diagram (modified after Deer et al., 1982) to validate the measured over-the-limits RI.

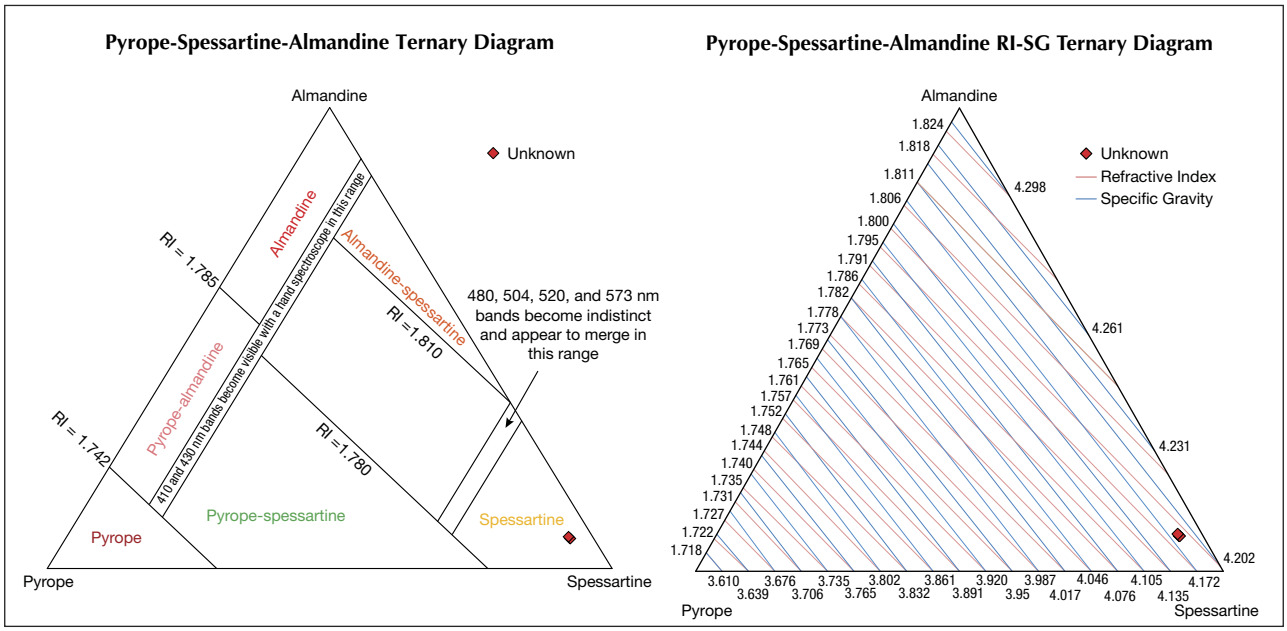

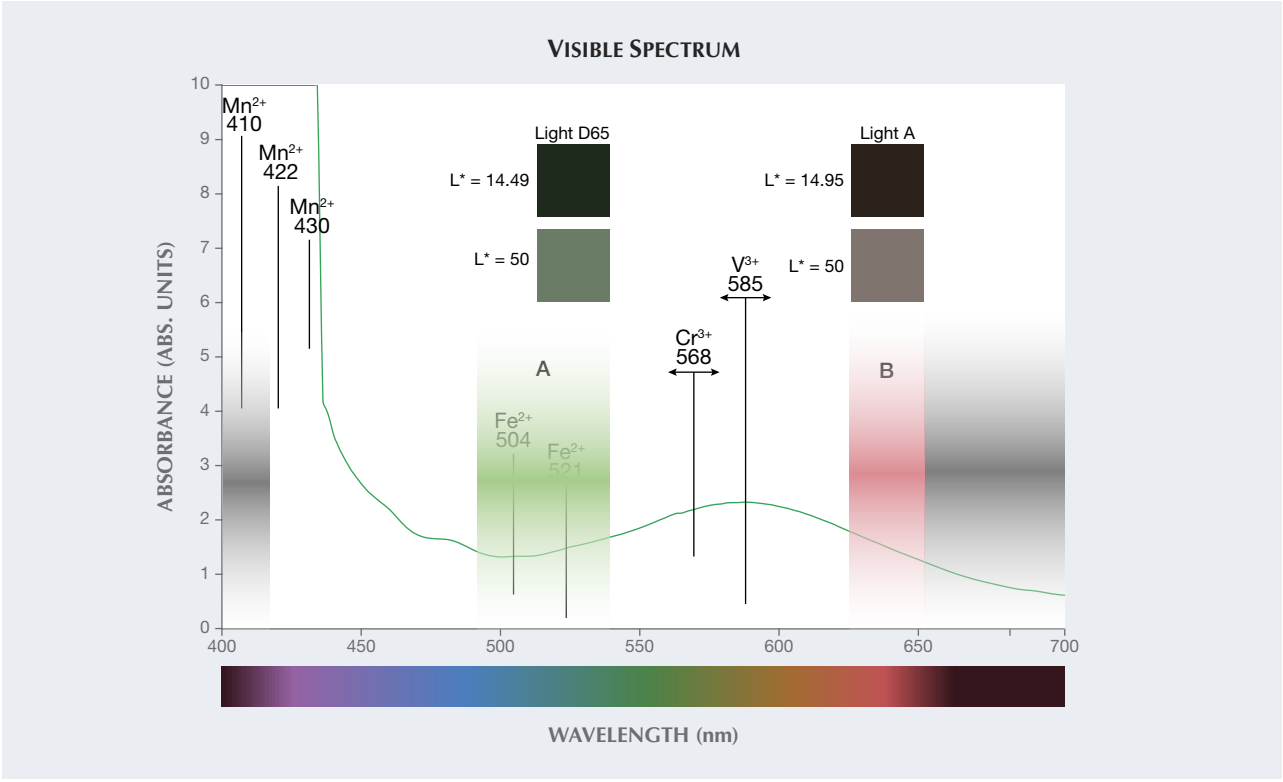

Figure 19. In the visible absorption spectrum of the stone, transmission window A is centered at 510 nm, while transmission window B is between 630 and 650 nm. The strong absorption below 450 nm is caused by Mn^{2+}; a wide absorption band between 550 and 650 nm is caused mainly by V^{3+}. The stone had so much Mn that the detector of the instrument was saturated below 440 nm. Calculated color pairs, representing the color of the stone seen under CIE D65 illumination and CIE A illumination, are shown above the two transmission windows. The human eye is not color sensitive above 650 nm or below 420 nm (both represented in the graph by the gray color zoning). The transmission in these wavelength ranges cannot be perceived effectively.

The calculated RI and SG—plotted in figure 18, right—were 1.797 and 4.182, respectively. The calculated RI value was consistent with the measured RI value. In 2001, Krzemnicki et al. reported a garnet composed of 76.9 mol.% spessartine and 4.2 mol.% goldmanite with a color change from orange-yellow under daylight-equivalent lighting to reddish orange under incandescent illumination based on the colorimetric data in the article, although color change from brownish green to brownish was observed visually ("Colour-change garnets from Madagascar: Comparison of colorimetric with chemical data," *Journal of Gemmology*, 2001, Vol. 27, No. 7, pp. 395–408). The high spessartine and goldmanite composition of the stone is similar to our stone reported here, but with much weaker color change.

To understand why this spessartine garnet showed a color-change phenomenon, we collected an ultraviolet/visible/near-infrared (UV-Vis-NIR) spectrum (the visible portion of the spectrum is shown in figure 19), which was then used to quantitatively calculate the stone's colorimetric coordinates (L*, a*, and b*; see table 2 at www.gia.edu/gems-gemology/summer-2019-labnotes-color-change-spessartine-garnet-icp-table2.pdf) under different lighting conditions. The strong absorption below 450 nm is caused by Mn^{2+} (R.K. Moore and W.B. White, "Electronic spectra of transition metal ions in silicate garnets," *Canadian Mineralogist*, Vol. 11, No. 4, 1972, pp. 791–811). A wide absorption band centered at about 585 nm is caused mainly by V^{3+} (C.A. Geiger et al., "Single-crystal IR- and UV/VIS-spectroscopic measurements on transition-metal-bearing pyrope: the incorporation of hydroxide in garnet," *European Journal of Mineralogy*, Vol. 12, No. 2, 2000, pp. 259–271), which produced two transmission windows: one in the blue-green part of the spectrum (figure 19, window A) and the other in the red (figure 19, window B). This was the cause of the color change in this spessartine garnet, as incandescent illumination highlighted the red transmission window and daylight-equivalent lighting highlighted the blue-green window. Color pairs under CIE D65 illumination (representing daylight-equivalent lighting) and CIE A illumination (representing incandescent illumination) were calculated and are shown in figure 19, above transmission window A and B. The darker color pair (top row), di-

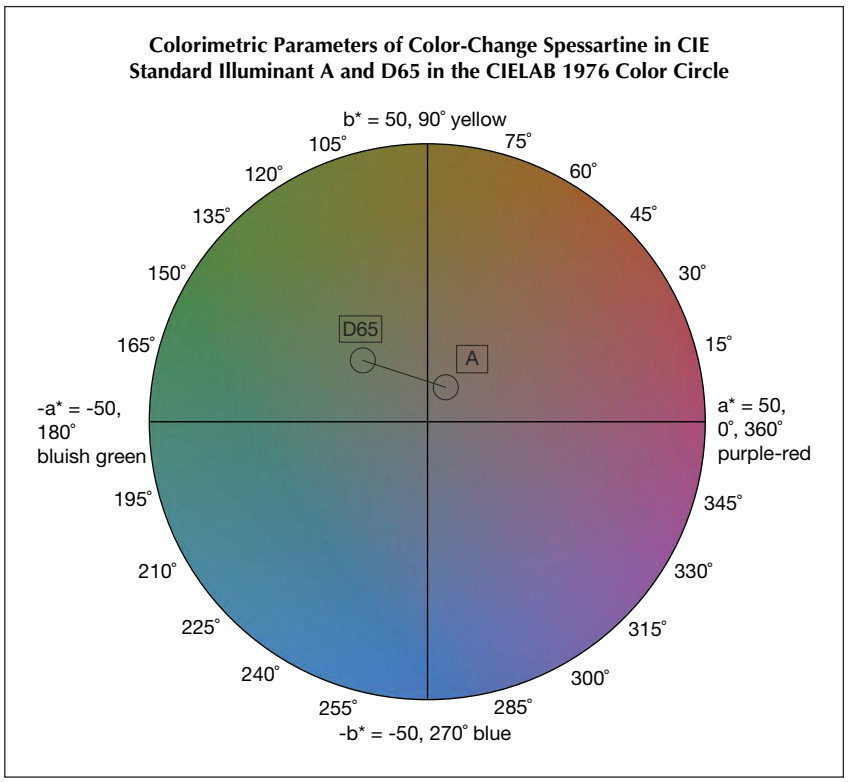

Figure 20. In the CIELAB 1976 color circle, the color of the stone changes from medium saturated green under CIE D65 illumination to low saturated orangy red under CIE A illumination, with a hue angle difference of 79.11°, a chroma difference of 9.25, and a color difference of 15.82. Full sets of L, a*, b* and RGB color coordinates are shown in table 2.*

rectly calculated from the measured UV-Vis-NIR spectrum, closely matched the dark appearance of the stone (again, see figure 17) with L* (lightness) around 14.5. It was the strong absorption generated by very high Mn and V concentration, along with the stone's relatively large size, that produced a long light path length. To better observe the saturation and hue of the color pair, the authors changed the L* to 50 and reproduced the color pair with the same a* and b* values (bottom row). The hue difference of the color pair is easier to see with increased lightness.

One way to judge the quality of a color-change stone is to plot the color pair in the CIELAB 1976 color circle. Good color-change pairings show a large hue angle difference, small chroma difference, and large chroma values (Z. Sun et al., "How to facet gem-quality chrysoberyl: Clues from the relationship between color and pleochroism, with spectroscopic analysis and colorimetric parameters," *American Mineralogist*, Vol. 102, No. 8, 2017, pp. 1747–1758). The color coordinates L*, a*, and b* (again, see table 2) of the stone under CIE D65 illumination and CIE A illumination were plotted in the CIELAB 1976 color circle in figure 20. The spessartine showed a low saturation under CIE A illumination.

Color change has been reported previously in pyrope-spessartine (K. Schmetzer et al., "Color-change garnets from Madagascar: Variation of chemical, spectroscopic and colorimetric properties," *Journal of Gemmology*, Vol. 31, No. 5-8, 2009, pp. 235–282), in pyrope (Z. Sun et al., "Vanadium- and chromium-bearing pink pyrope garnet: characterization and quantitative colorimetric analysis," Winter 2015 *G&G*, pp. 348–369), and in grossular (Spring 2018 GNI, pp. 233–236). To the authors' knowledge, this was the first color-change spessartine reported.

Heidi Breitzmann, Ziyin Sun, and Aaron C. Palke

SPURRITE

Recently, a 19.68 ct gray-purple stone (figure 21) was submitted to the Carlsbad laboratory for identification. The square cabochon was semi-translucent and had wispy white features throughout.

It had a refractive index of 1.68–1.64 and a hydrostatic specific gravity of 3.00. Raman spectroscopy identified it as spurrite (figure 22), which aligned with the gemological properties already measured. Spurrite is a nesosilicate with a chemical composition of $Ca_5(SiO_4)_2CO_3$ (J.W. Anthony et al., *Handbook of Mineralogy*, Vol. 2, Mineral Data Publishing, 1995). Analysis by energy-dispersive X-ray fluorescence (EDXRF) showed high amounts of calcium and silicon.

Figure 21. A 19.68 ct gray-purple spurrite that was submitted to GIA's Carlsbad lab.

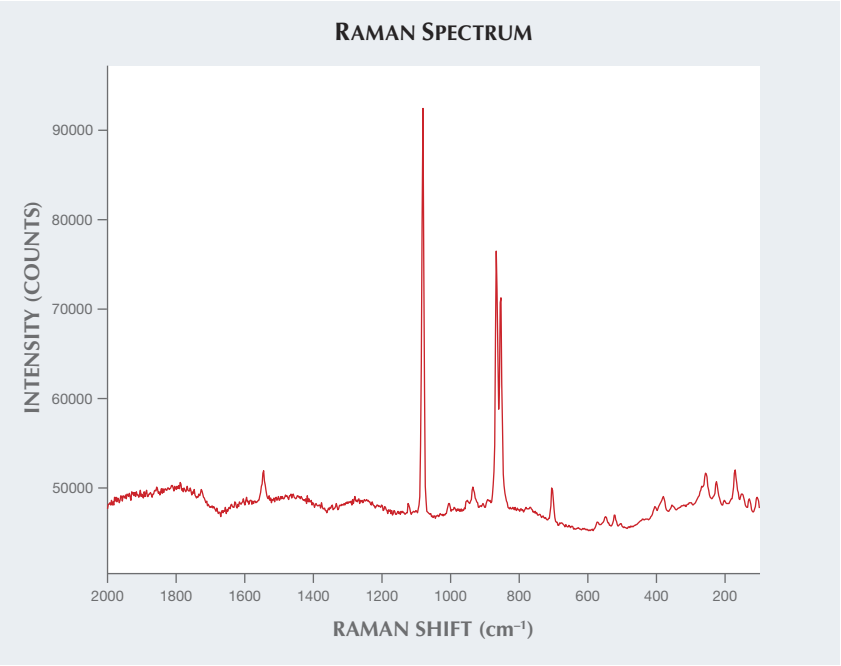

Figure 22. Raman spectroscopy identified the gray-purple stone as spurrite.

Spurrite occurs in high-temperature thermal metamorphism along the contact between carbonate rock and mafic magma (Anthony et al., 1995). A common inclusion found within spurrite is black metallic magnetite crystals. Raman spectroscopy identified the metallic opaque inclusions that broke the surface (figure 23) as magnetite (figure 24), further evidence that this stone was a spurrite.

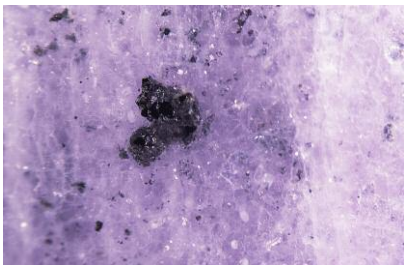

Figure 23. Magnetite, identified using Raman spectroscopy, breaks the surface of the spurrite. Field of view 4.79 mm.

Encountering stones that require more research and a little detective work, such as this spurrite, can enhance one's curiosity about gemology.

Nicole Ahline

Figure 24. Raman spectroscopy identified the inclusion in the spurrite as magnetite.

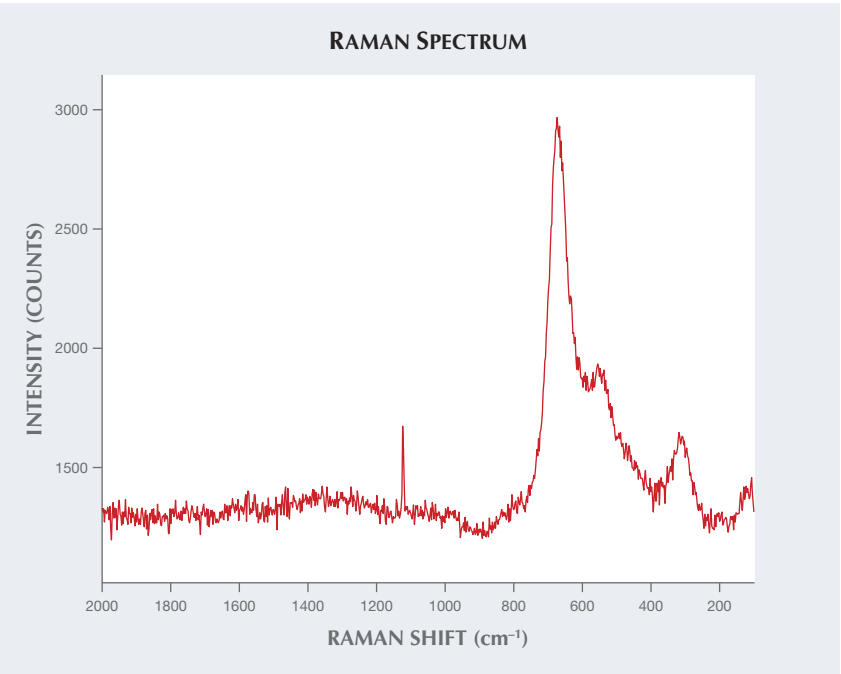

Exsolved Particles with Natural Appearance Within Flux-Grown Pink SYNTHETIC SAPPHIRE

The Carlsbad laboratory recently examined unusual exsolved flux particles in a flux-grown pink synthetic sapphire. The specimen, mounted in a ring, had an estimated weight of 13.07 ct and a refractive index of 1.760–1.770. It displayed a typical pink sapphire spectrum with a hand-held spectroscope. Strong red fluorescence was seen under both long-wave and short-wave UV. Laser ablation–inductively coupled plasma–mass spectrometry (LA-ICP-MS) detected high levels of platinum; the concentrations of iron, beryllium, titanium, vanadium, and gallium were either below the detection or quantification limit.

Microscopic examination revealed further evidence of a synthetic origin: a single reflective platinum platelet with negative hexagonal growth through the center (figure 25, left). Also observed were interconnected channels of exsolved flux creating fingerprints (figure 25, right).

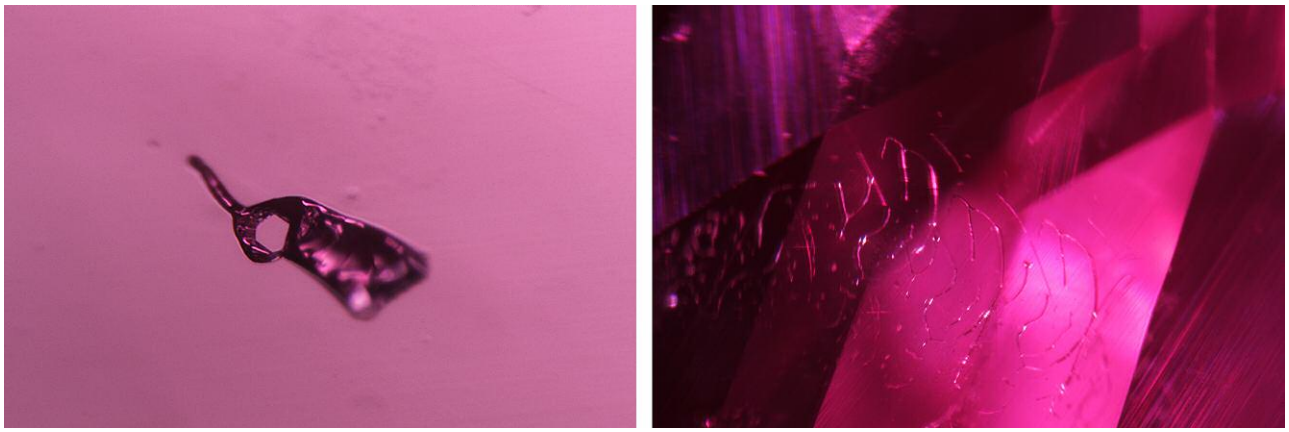

Figure 25. Left: Reflective platinum platelet with negative hexagonal growth within a flux-grown pink synthetic sapphire; field of view 2.34 mm. Right: Channels of exsolved interconnected flux; field of view 4.79 mm.

A potentially challenging inclusion was seen in the form of minute rounded flux particles aligned in organized linear rows (figure 26), which displayed a striking resemblance to fingerprints and silk clouds commonly seen within natural corundum. These particles were observed in relative abundance at varying depths. Grid-like exsolved solid inclusions have been mentioned in the literature as possible properties of synthetic corundum (R.W. Hughes et al., *Ruby & Sapphire: A Gemologist's Guide*, Lotus RWH Publishing, Bangkok, 2017). It has not been stated how abundant these natural-looking fingerprints are within flux-grown synthetic material, but this type of inclusion is rarely seen at the Carlsbad laboratory. Identifying the natural or synthetic origin of a stone with this type of natural-looking inclusion can be challenging. If a gem material is suspected of being synthetic, it is advisable to submit it to a gemological laboratory.

Figure 26. Fine rounded flux particles aligned into linear stringers resembling fingerprints and silk clouds seen within natural corundum; field of view 1.73 mm.

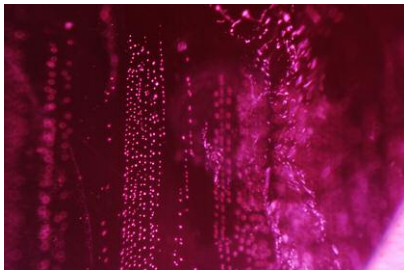

Britni LeCroy

PHOTO CREDITS
Robison McMurtry—1, 17, 21; Michaela Stephan—2, 3 (left); Diego Sanchez—4, 7, 9, 15, 17; Nathan Renfro—5; Nuttapol Kitdee—11; Kwanreun Lawanwong—12, 13, 14; Promlikit Kessrapong—13; Jessa Rizzo—16; Nicole Ahline—23; Britni LeCroy—25, 26

For More on Lab Notes

X ray computed microtomography (μ CT) imaging reveals a hollow pearl filled with foreign material. View the videos at www.gia.edu/gems gemology/summer 2019 labnotes hollow pearl filled with foreign material